It will be interesting to see whether future studies reveal exceptional compositions in other meteorites. A suitable starting point in the search for such objects would be meteorites that are similar to Butler in Ni content and structure. The Prior-Hey catalog indicates that Tazewell, Cowra, Laurens County, and Victoria West might be suitable. We have studied the first two of these objects and find that they are anomalous in the sense that they are not members of the known Ga-Ge groups, but do not show exceptional metal/Ni ratios. We plan to study the latter two objects as soon as samples can be obtained.

JOHN T. WASSON
Department of Chemistry and
Institute of Geophysics and Planetary Physics, University of California, Los Angeles 90024

References and Notes

1. G. C. Broadhead, *Amer. J. Sci.* **110**, 401 (1875).
2. A. Brezina, *Sitzsber. Akad. Wiss. Wien, Math.-Naturw. Kl.* **82**, 348 (1880); E. Cohen, *Meteoritenkunde* (Schweizerbart'sche Verlagshandlung, Stuttgart, 1905), vol. 3, pp. 281–284.
3. G. T. Prior and M. H. Hey, *Catalogue of Meteorites* (British Museum, London, 1953).
4. J. L. Smith, *Amer. J. Sci.* **113**, 213 (1877).
5. V. F. Buchwald and S. Munck, *Analecta Geologica* **1**, 1 (1965).
6. S. H. Perry, *The Metallography of Meteoritic Iron*, Bull. No. 184 (U.S. National Museum, Washington, D.C., 1944) p. 132; A. Brezina, *Denkschr. Math.-Naturwiss Kl. Akad. Wiss. Wien.* **44**, 134 (1881).
7. E. Goldberg, A. Uchiyama, H. Brown, *Geochim. Cosmochim. Acta* **2**, 1 (1951); J. F. Lovering, W. Nichiporuk, A. Chodos, H. Brown, *ibid.* **11**, 263 (1957).
8. W. Nichiporuk and H. Brown, *J. Geophys. Res.* **70**, 459 (1965).
9. J. T. Wasson and J. Kimberlin, *Radiochim. Acta* **5**, 170 (1966); ———, P. K. Mattschei, E. Groszek, *Trans. Amer. Geophys. Union* **47**, in press.
10. J. T. Wasson, *Geochim. Cosmochim. Acta*, in press.
11. ——— and J. Kimberlin, *J. Geophys. Res.* in preparation.
12. J. C. Cobb and G. Moran, *ibid.* **70**, 5309 (1965); M. Shima, *Geochim. Cosmochim. Acta* **28**, 517 (1964); A. A. Smales, D. Mapper, J. W. Morgan, R. K. Webster, A. J. Wood, *Proc. U.N. Intern. Conf. Peaceful Uses At. Energy 2nd Geneva* **2**, 242 (1958).
13. J. T. Wasson and G. W. Wetherill, in preparation; J. T. Wasson, *Rev. Geophys.*, in press.
14. The ten elements are Ga, Ge, Ru, Rh, Pd, Re, Os, Ir, Pt, and Au.
15. J. I. Goldstein, *Science*, this issue.
16. I am indebted to J. Kimberlin for his assistance in this research. Dr. U. Marvin and Professor C. Frondel have generously supplied a sample of Butler. This investigation was supported in part by NASA grant NSG 237-62 and by NSF grant GP-5309.

28 March 1966

Stokes Parameters for 1665-Megacycles-per-second Emission from OH near Source W3

Abstract. *The Stokes parameters were measured as a function of frequency for the anomalous 1665-megacycles-per-second OH emission originating near the thermal radio source W3. The emission is highly polarized, and the polarization parameters vary rapidly with frequency. The observed polarization can be described in terms of narrow, roughly Gaussian, emission features, all with uniform polarization but with several features overlapping without coherence near the center of the spectrum. Most of the individual features may be 100-percent polarized. Detailed examination of the brightest features suggest that they are not exactly Gaussian in shape.*

The anomalous 1665-Mc/sec spectral line emission from OH near source W3 has been observed to be partially linearly polarized (*1*). Subsequent observations of right and left circular polarization from this source (*2*) revealed that all four of the OH transitions at 1612, 1665, 1667, and 1720 Mc/sec produce features in the emission spectrum with predominantly circular polarization. Linear and circular polarization in the 1665 Mc/sec emission from the W3 source have also been observed (*3*).

We now report measurement of the Stokes parameters as a function of frequency for the 1665-Mc/sec OH emission near W3. The polarization parameters—ellipticity, ellipse position angle, and degree of polarization—are computed, and their rapid variation with frequency is described in terms of a simple model.

The polarization properties of an electromagnetic wave are completely specified by the four Stokes parameters (*4*), which may be determined from measurements of the intensities of the wave with four independent polarizations. If $I(\phi)$ is the intensity for linear polarization at a position angle ϕ, and if $I(\mathrm{R})$ and $I(\mathrm{L})$ are the intensities for right and left circular polarization (*5*), then the Stokes parameters are defined:

$$\begin{aligned} S_0 &= I(0°) + I(90°) = I(\mathrm{R}) + I(\mathrm{L}) \\ S_1 &= I(0°) - I(90°) \\ S_2 &= I(45°) - I(135°) \\ S_3 &= I(\mathrm{R}) - I(\mathrm{L}). \end{aligned} \quad (1)$$

These parameters have such a property that the polarization of an incoherent superposition of waves is described by Stokes parameters which are just the sums of respective parameters for the separate waves. Other parameters describing the polarization can be obtained from the Stokes parameters thus: The position angle ϕ of the major axis of the polarization ellipse is given by

$$\tan(2\phi) = S_2/S_1 \quad (2)$$

The amplitude ratio of minor to major axes, b/a, for the polarization ellipse is expressed as

$$\tan x = \pm\, b/a \quad (3)$$

where

$$\sin 2x = S_3/\sqrt{S_1^2 + S_2^2 + S_3^2} \quad (4)$$

and the plus sign in Eq. 3 applies to right elliptical, and the minus sign to left elliptical, polarization. Finally the degree of polarization P is obtained from

$$P = \sqrt{S_1^2 + S_2^2 + S_3^2}\ /S_0 \quad (5)$$

It is convenient to work with the Stokes parameters because of their additive property, but the ellipse position angle ϕ, the ellipticity $\pm b/a$, and the degree of polarization P, as we have defined them, yield somewhat better physical insight.

Polarization parameters for the 1665-Mc/sec OH emission were measured with a 120-foot (37-m) parabolic antenna (*6*) between 28 November and 9 December 1965. Observation of various linear and circular polarizations with a single system enabled complete determination of the polarization parameters of the spectral features as functions of frequency, or, equivalently, as functions of radial velocity relative to the local standard of rest. At this OH-transition frequency a radial velocity of +1 km/sec gives a Doppler shift of −5.555 kc/sec.

The spectral-line radiometer used for these measurements included a 100-channel digital autocorrelator and a room-temperature parametric amplifier. The autocorrelator was tied directly to a real-time computer which produced plots of the observed spectra immediately after each integration period. Most of the observations were made with a 1-kc/sec frequency resolution, but the brightest features were also examined with 200-cy/sec resolution. The overall system temperature was 320°K for linear-polarization measurements and 360°K for circular polarization. The increased system temperature resulted from a network that combined horizontal and vertical linear polariza-

tion to produce the circular polarizations. The observed antenna temperatures for Cassiopeia A continuum emission were 240° and 180°K for linear and circular polarization, respectively. The isolation of right and left circular polarization was greater than 15 db, and the half-power beam width was 22 minutes of arc.

The spectral line measurements consisted in part of a series of 30-minute integrations, each covering a spectral width of 40 kc/sec with an equivalent filter width of 1 kc/sec. Two 40-kc/sec windows, overlapping in frequency, were used to measure the 1665-Mc/sec emission spectrum of the W3 source over a total spectral width of 64 kc/sec; thus the central interval, 16-kc/sec wide, received twice the integration time of the outer intervals. All measurements were made by comparing the antenna temperature with a room-temperature load. The linear-polarization measurements were made with horizontal polarization, and the variation of position angles was provided by earth rotation, which gave more or less uniform coverage over a 225°-interval of position angles during the observation period. The linear-polarization measurements were made between 28 and 30 November 1965 between 2000 and 0600 hours E.S.T. No corrections were made for Faraday rotation, on which the upper limit at OH frequencies, based on radar-lunar measurements (*7*), is about 5° during daylight hours; at night it should be smaller by a factor of one-third or one-sixth.

The data from each spectral measurement consisted of 161 values of the antenna temperature corresponding to equally spaced Doppler frequency offsets relative to the local standard of rest. If T_{ij} represents the antenna temperature for the i^{th} spectrum ($1 \leq i \leq N$) with frequency offset $\Delta\nu_j$, then the determinations of S_0 and S_3 from circular-polarization measurements follow from Eq. 1:

$$S_0(\Delta\nu_j) = N^{-1}\sum_{i=1}^{N}[T_{ij}(\mathrm{R}) + T_{ij}(\mathrm{L})] \quad (6)$$

$$S_3(\Delta\nu_j) = N^{-1}\sum_{i=1}^{N}[T_{ij}(\mathrm{R}) - T_{ij}(\mathrm{L})] \quad (7)$$

The linear measurements were reduced by the method of least squares so that

$$\sum_{i=1}^{N}[T_{ij}(\phi_i) - \mathrm{A}_j - \mathrm{B}_j\cos 2(\phi_i - \phi_j)]^2 = \text{minimum} \quad (8)$$

Table 1. Parameters for 1665-Mc/sec OH emission features. Radial velocities are relative to the local standard of rest.

Radial velocity (km/sec)	Maximum T_A (°K)	Width, half-max. (km/sec)	Ellipticity ($\pm b/a$)	Ellipse position angle (deg)	Polarization (%)	Comment
−49.13	11.0	0.27	−0.75(±.1)	170(±30)	51(±3)	Isolated feature
−46.39	28.0	.68	− .93(±.07)	10(±10)	100(−6)	Slightly overlapped feature
−45.42	35.0	.55	− .84	65	100	Parameters from model
−45.13	50.0	.45	+ .65	55	100	Parameters from model
−44.55	16.0	.50	− .70	105	100	Parameters from model
−43.73	30.0	.35	+ .78(±.06)	165(±10)	86(±6)	Slightly overlapped feature
−43.08	8.0	.26	+ .78(±.2)	90(±14)	100(−20)	Isolated feature
−41.73	14.0 (±0.5 RMS)	.36 (±.05)	+ .96(±.04)	110(±30)	100(−12)	Isolated feature

In this way the three parameters A_j, B_j, and ϕ_j were determined for each frequency offset $\Delta\nu_j$, and with this determination of the linear polarization one could reconstruct the remaining Stokes parameters $S_1(\Delta\nu_j)$ and $S_2(\Delta\nu_j)$, as well as obtain a redundant measurement of S_0 (*8*).

This complete analysis was performed with a digital computer that used magnetic-tape recordings of the observed spectra as input. The root-mean-square (RMS) errors in the Stokes parameters were computed by taking independent samples of the baseline fluctuations at the high- and low-frequency ends of the computed $S_k(\Delta\nu_j)$. It should be remembered that these estimates are conservative for the central portion of the spectra where the integration time, as previously noted, is twice as long.

Figure 1, *a* and *b*, shows the Stokes parameters plotted as a function of radial velocity, with the RMS errors and frequency resolution specified. In Fig. 1*b* the antenna temperature scale is expanded by a factor of two from that in Fig. 1*a*. It is clear from these curves that the polarization is primarily circular, progressing from totally right circular on the right side of Fig. 1*a* to totally left circular for the feature just to the left of the central maximum. Figure 1*b* shows that the amount of linear polarization is relatively small by comparison. The polarization behavior across the central maximum is evidently very complex.

Once the Stokes parameters have been determined, it is desirable to use them to compute the ellipticity, the ellipse position angle, and the degree of polarization for the emission spectrum. These last three parameters, however, are not proportional to the received signal and can be determined only when the signal:noise ratio is sufficiently high.

Equations 3–5 were used to compute the ellipticity $\pm b/a$ and the degree of polarization P. The ellipse position angle ϕ was determined as a parameter in the least-squares fitting procedure (Eq. 8). The RMS errors associated with these three parameters were computed by estimating the RMS errors in the Stokes parameters and assuming linear error propagation. The polariza-

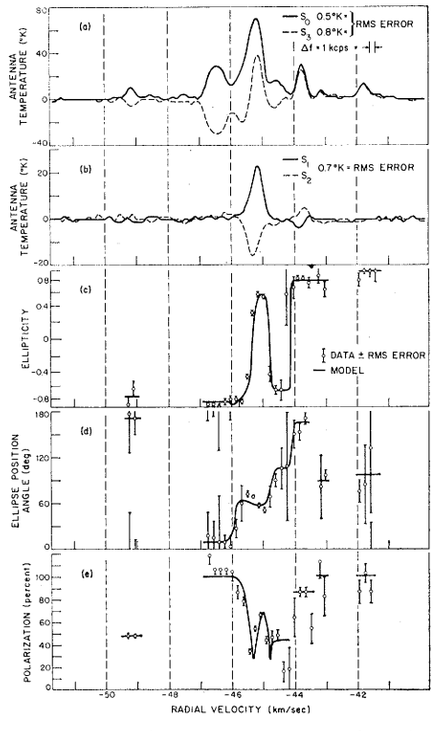

Fig. 1. Polarization parameters for the 1665-Mc/sec OH emission near W3. *a* and *b*, Measured values of the Stokes parameters. The points plotted in *c*, *d*, and *e* were computed from the Stokes parameters. Solid lines represent values derived from the model from −46 to −44 km/sec, or best estimates (otherwise derived) of the parameters.

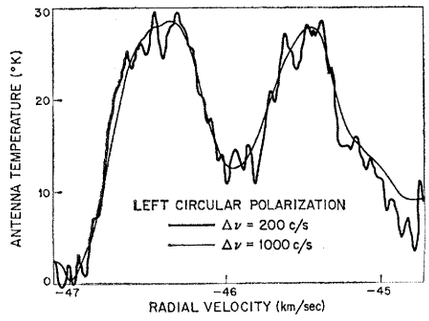

Fig. 2. The OH spectra of two bright features observed with high resolution.

tion parameters and the RMS error bars are shown in Fig. 1, *c*, *d*, and *e*. The plotted points here are separated by an equivalent filter width in frequency, so they represent independent measurements. The large errors are associated with low signal:noise ratios, and no points are plotted when the errors become excessive.

The polarization parameters in Fig. 1 show continuous variation around the central maximum, but outside this region of variability the polarization parameters appear to remain constant, within experimental error, across the individual emission features. We have used a simple model to describe the variability of the polarization parameters in the region of the central maximum. This model assumes that there are three incoherent emission features in the radial-velocity interval −46 to −44 km/sec. These features are assumed to be 100-percent polarized and to have Gaussian profiles. The polarization variability then results from incoherent superposition. The problem of fitting this model to the observed polarization parameters in the region of the central maximum is not simple. Five parameters are necessary to specify the center frequency, width, peak intensity, and polarization of each feature. These parameters were obtained by repeated trial and error with a computer program that combined trial values of the Stokes parameters in this model and plotted the resulting polarization parameters, with the observed data superimposed. The solid curves in Fig. 1, *c*, *d*, and *e*, show the best fit obtained by this procedure. The parameters that produced this fit are given in Table 1, which also includes the corresponding parameters for all features in the spectrum shown in Fig. 1. The overall agreement is good between the observed data and the model in Fig. 1, *c*, *d*, and *e*, but the small discrepancies may be large compared with the RMS error bars on the data points. We believe that these discrepancies result from the following causes: (i) the features are not exactly Gaussian in shape; (ii) the resolution of 1 kc/sec is not quite sufficient to resolve completely the spectrum of the source; and (iii) the cut-and-try fitting procedure did not produce the best-fit parameters. In general, this simple model does indeed appear to fit the observed variations in polarization parameters.

Outside the interval −44 to −46 km/sec, in which an overlap of 100-percent polarized features is assumed to account for $P < 1$, only two of the remaining five features are significantly less than 100-percent polarized. The feature at −49.1 km/sec is 51-percent polarized (± 3 RMS error) and the feature at −43.7 km/sec is 86-percent polarized (± 6 RMS error).

It has been proposed (*3*) that the Zeeman effect may account for this spectrum, but the identification of Zeeman components suggested does not appear consistent with our observed polarization parameters and the results in Table 1. We cannot, of course, say on the basis of our measurement that no combination of simple Zeeman components can produce the observed spectrum for the 1665-Mc/sec transition. But the circular-polarization observations of the other three OH transitions from the W3 source by Barrett and Rogers (*2*) appear to rule out a simple interpretation of this 1665-Mc/sec spectrum in terms of Zeeman splitting.

The attempt (just described) to fit the observed spectra with Gaussian features disclosed small but significant deviations from a best-fit Gaussian curve. In particular, the bright feature centered at −46.4 km/sec showed uniform polarization parameters but could not be fitted exactly with a Gaussian. To examine the shape in more detail, the spectrum from −45 to −47 km/sec was observed with a resolution of 200 cy/sec, with left circular polarization; Fig. 2 shows the resulting spectrum, with the 1-kc/sec spectrum superimposed. The two features in this figure appear to be well-resolved with the larger equivalent filter width. The agreement is consistent with the expected RMS fluctuations in the 200-cy/sec data, but the feature shape from −47 to −46 km/sec is significantly non-Gaussian; it has an asymmetric peak and falls off much more rapidly around −47 km/sec than a Gaussian with the observed width at half maximum. Possibly, of course, this feature may be decomposed into two or more Gaussians, but the observed 100-percent polarization requires that all features in the decomposition have the same polarization parameters.

The spectrum of the 1665-Mc/sec OH transition observed near W3 shows the bright, narrow, emission features that are characteristic of the anomalous emission associated with interstellar gas clouds near H II regions. Detailed examination of the polarization parameters shows that the spectrum can be interpreted as an incoherent superposition of emission features, each with polarization parameters that are constant across the feature. The features are roughly Gaussian in shape, but with some significant deviations. Altogether eight features appear to be present in the spectrum, but some additional low-level emission may be present, particularly in the interval −49 to −47 km/sec. Three emission features are 100-percent polarized within the observational errors. Three other features, which overlap in frequency, are consistent with a model in which the features themselves are 100-percent polarized and the observed degree of polarization is a consequence of an incoherent superposition. The two remaining features are not obviously overlapped yet give $P < 1$; however, some overlap with low-level emission may be present. Generally the observations are consistent with a superposition of 100-percent polarized features that are mutually incoherent. The observed polarization varies continuously from left circular, through linear to right-hand elliptical, and back to left-hand elliptical between radial velocities of −46 and −44 km/sec. The model simulates this behavior with features that are elliptical, with ellipticity $|b/a| \geq 0.65$, or equivalently with linear polarization amounting to 41 percent or less.

The mechanism producing these features is not clearly understood. However, the description of the emission in terms of our simple model enables the conclusion that the 1665 Mc/sec emission near W3 is not qualitatively different from that of the other three transitions, notwithstanding the observed variations in the polarization parameters as a function of radial velocity.

The deviations from Gaussian shape may be a consequence of the line-narrowing characteristic of maser amplification processes in which saturation occurs (*9*). Several schemes for obtaining population inversion of the appro-

priate OH energy levels have been proposed (*10, 11*); the only one that leads directly to circular and elliptical polarization is that of Litvak *et al.* (*11*).

M. L. MEEKS, J. A. BALL
J. C. CARTER, R. P. INGALLS
Lincoln Laboratory, Massachusetts Institute of Technology, Lexington

References and Notes

1. S. Weinreb, M. L. Meeks, J. C. Carter, A. H. Barrett, A. E. E. Rogers, *Nature* **208**, 440 (1965).
2. A. H. Barrett and A. E. E. Rogers, *ibid.* **210**, 188 (1966).
3. R. D. Davies, G. de Jager, G. L. Verschuur, *ibid.* **209**, 974 (1966).
4. M. Born and E. Wolf, *Principles of Optics* (Pergamon, New York, 1959), p. 550.
5. Right-hand circular polarization denotes clockwise rotation of the electric vector when viewed along the direction of propagation.
6. Of the Haystack Research Facility of Lincoln Laboratory, M.I.T.
7. G. H. Millman, *J. Geophys. Res.* **69**, 429 (1964).
8. The parameter S_0 may be determined from $S_0 = 2A$ as well as from Eq. 6. This independent determination was made, and was checked against the sum of right and left circular, to verify the computational procedure and the calibration of the linear and circular feeds.
9. G. Birnbaum, *Optical Masers* (Academic Press, New York, 1964), p. 34.
10. J. L. Symons, *Nature* **208**, 1195 (1965); B. Turner, private communication; A. H. Cook, *Nature* **210**, 611 (1966); F. Perkins, T. Gold, E. E. Salpeter, "Report CSUAC 40," Cornell–Sydney University Astronomy Center, Ithaca, N.Y., March 1966.
11. M. M. Litvak, A. L. McWhorter, M. L. Meeks, H. J. Zeiger, in preparation.
12. We thank A. E. E. Rogers, G. H. Conant, Jr., and the staff of Haystack Research Facility for assistance. Lincoln Laboratory is operated by M.I.T. with the support of the U.S. Air Force.

16 June 1966

Implantation in Interplanetary Dust of Rare-Gas Ions from Solar Flares

Abstract. *Measurements of excess Ar^{36} + Ar^{38} (released mainly at 1200°C) in magnetic concentrates of Pacific sediments and in a dense concentrate of Greenland dust agree within an order of magnitude with expected concentrations implanted by solar-flare ion streams of energy less than 10 Mev per atomic-mass unit. The agreement implies that more than 10 percent of each concentrate may be extraterrestrial, depending on size distribution and flare spectra. Rare-gas measurements on fine-grained dust can provide data on: solar-flare "paleo-ion" fluxes, energy spectra, and isotopic abundances; identification, mineralogy, and chemistry of interplanetary dust; influx rates to Earth and sedimentation rates of oceanic cores; and lunar-surface residence and mixing times.*

An approximation of the flux of solar-flare protons in interplanetary space was derived from measurements of Al^{26} in oceanic sediments (*1*). Measurements of solar-flare ions stopped in extraterrestrial material are an alternative source of information about average flare ion fluxes in space, and the rare gases are ideally suited for this purpose. I shall summarize some recent mass-spectrometric measurements bearing on this problem, present calculations of expected concentrations of the rare gases implanted from a solar-flare source, and compare observed concentrations with expected values.

Figure 1 presents measured Ar^{40}: Ar^{36} ratios found in argon released during successive 1-hour heatings from four concentrates—three magnetic concentrates of a Pacific red clay and a high-density concentrate ($\rho > 3.2$) of particulate matter from Greenland ice. The solid line represents Merrihue's initial discovery of a red-clay concentrate with Ar^{40} : Ar^{36} lower than the value of 296 found in air (*2*). All the concentrates have argon, released at one or more temperatures, with an Ar^{40} : Ar^{36} ratio of 235 or less; the argon from each appears to be a mixture of radiogenic Ar^{40} from potassium, excess Ar^{36} + Ar^{38}, and atmospheric argon (*2, 3*).

At all temperatures with observable Ar^{40} : Ar^{36} anomalies, the Ar^{36} : Ar^{38} ratio was indistinguishable from that in air. There is no strong positive evidence of argon or other rare-gas isotopic anomalies produced by cosmic ray–spallation nuclear reactions in any of the concentrates. The apparent minimum excesses of Ar^{36} and Ar^{36} + Ar^{38} have been calculated (Table 1) and are strikingly similar.

Table 1. Minimum excess argon, assuming that all Ar^{40} is atmospheric whenever Ar^{40}: Ar^{36} is less than the ratio in air, that there is no excess Ar^{36} whenever Ar^{40}: Ar^{36} exceeds the ratio in air, and that Ar^{36}: Ar^{38} equals the ratio in air.

Minimum excess argon (10^{-10} cm^3g^{-1} at STP)	
Ar^{36}	Ar^{36} + Ar^{38}
Three marine sediments (magnetic fraction)	
7 (*2*)	8 (*2*)
8	9.5
6	7
Greenland dust (dense fraction: $\rho > 3.2$)	
8	11

Table 2 compares data on He^4 and Ne^{20} released from the dense Greenland sample with similar findings by Merrihue in a magnetic sample of Pacific sediment (*2*). The range of 20 to 40 mg/cm^2 for α-particles emitted by nuclides in the U and Th decay chains will cause loss of radiogenic He^4 from small grains. The K-A age of the Greenland concentrate is 25 times greater than that of the sea-sediment concentrates, yet the latter are the richer in He^4. Although there is no positive evidence of correlation of He^4 concentration with apparent age, U and Th have not been measured. Here we shall neglect radiogenic He^4.

The He^4:Ne^{20} ratios at 500° to 600°C are approximately the same as the relative "cosmic" abundances. The evident similarities of amounts of excess argon, of high-temperature argon isotopic ratios, and of amounts of 500°C helium and neon all emphasize the worldwide occurrence of the rare-gas abundance patterns.

No terrestrial samples having this pattern of rare-gas abundances or these subatmospheric Ar^{40} : Ar^{36} ratios have yet been found; nor is there a plausible terrestrial mechanism for explaining these observations. Three extraterrestrial mechanisms have been suggested (*2, 3*) to explain these observations in fine-grained material from low-accumulation locations. A solar flare source was one such suggestion.

The only mineral detectable in common by x-ray diffraction in concentrates from both geographic locations is magnetite. Fine-grained magnetite is a plausible extraterrestrial material (*4*), and sufficiently fine-grained material of low velocity (*5*) penetrates the atmosphere without melting. In view of the lack of major isotopic fractionation of excess Ar^{36} and Ar^{38}, and the lack of major elemental fractionation be-

Table 2. Releases of He^4 and Ne^{20} at various temperatures.

T (100°C)	Release (cm^3g^{-1} at STP)		He^4: Ne^{20}
	He^4 ($\times 10^{-6}$)	Ne^{20} ($\times 10^{-8}$)	
	Greenland dense, $\rho > 3.2$		
5	5.2	1.2	420
8	0.94	7.0	13
10	.07	7.0	1
12	< .01	5.0	< 0.2
	Pacific magnetic (2)		
6	6.1	1.3	470
10	9.1	4.0	230
14	0.29	1.0	29